Overview of the FTU results

View the article online for updates and enhancements.

Recent citations

Overview of the FTU results

G. Pucella[1]**, E. Alessi**[2]**, B. Angelini**[1]**, M.L. Apicella**[1]**, G. Apruzzese**[1]**,
G. Artaserse**[1]**, B. Baiocchi**[2]**, F. Belli**[1]**, W. Bin**[2]**, F. Bombarda**[1]**, L. Boncagni**[1]**,
A. Botrugno**[1]**, S. Briguglio**[1]**, A. Bruschi**[2]**, P. Buratti**[1]**, G. Calabrò**[1]**,
M. Cappelli**[1]**, A. Cardinali**[1]**, D. Carnevale**[3]**, L. Carraro**[4]**, C. Castaldo**[1]**,
F. Causa**[2]**, S. Ceccuzzi**[1]**, C. Centioli**[1]**, R. Cesario**[1]**, C. Cianfarani**[1]**, G. Claps**[1]**,
V. Cocilovo**[1]**, F. Cordella**[1]**, F. Crisanti**[1]**, O. D'Arcangelo**[1]**,
M. De Angeli**[2]**, C. Di Troia**[1]**, B. Esposito**[1]**, F. Fanale**[2]**, D. Farina**[2]**, L. Figini**[2]**,
G. Fogaccia**[1]**, D. Frigione**[1]**, V. Fusco**[1]**, L. Gabellieri**[1]**, S. Garavaglia**[2]**,
E. Giovannozzi**[1]**, G. Gittini**[2]**, G. Granucci**[2]**, G. Grosso**[2]**, M. Iafrati**[1]**,
F. Iannone**[1]**, L. Laguardia**[2]**, E. Lazzaro**[2]**, M. Lontano**[2]**, G. Maddaluno**[1]**,
S. Magagnino**[1]**, M. Marinucci**[1]**, D. Marocco**[1]**, G. Mazzitelli**[1]**, C. Mazzotta**[1]**,
V. Mellera**[2]**, A. Milovanov**[1]**, D. Minelli**[2]**, F.C. Mirizzi**[5]**, A. Moro**[2]**, S. Nowak**[2]**,
D. Pacella**[1]**, F. Pallotta**[2]**, L. Panaccione**[5]**, M. Panella**[5]**, V. Pericoli-Ridolfini**[5]**,
A. Pizzuto**[1]**, S. Podda**[1]**, M.E. Puiatti**[4]**, G. Ramogida**[1]**, G. Ravera**[1]**, D. Ricci**[2]**,
A. Romano**[1]**, A. Simonetto**[2]**, C. Sozzi**[2]**, U. Tartari**[2]**, A.A. Tuccillo**[1]**,
O. Tudisco**[1]**, M. Valisa**[4]**, B. Viola**[1]**, E. Vitale**[1]**, G. Vlad**[1]**, B. Zeniol**[4]**,
M. Zerbini**[1]**, F. Zonca**[1]**, M. Aquilini**[1]**, P. Cefali**[1]**, E. Di Ferdinando**[1]**,
S. Di Giovenale**[1]**, G. Giacomi**[1]**, A. Grosso**[1]**, M. Mezzacappa**[1]**, A. Pensa**[1]**,
P. Petrolini**[1]**, V. Piergotti**[1]**, B. Raspante**[1]**, G. Rocchi**[1]**, A. Sibio**[1]**, B. Tilia**[1]**,
R. Tulli**[1]**, M. Vellucci**[1]**, D. Zannetti**[1]**, S. Almaviva**[1]**, F. Bagnato**[6]**, G. Brolatti**[1]**,
A. Buscarino**[7]**, L. Calacci**[3]**, L. Caneve**[1]**, M. Carlini**[8]**, F. Colao**[1]**, C. Corradino**[7]**,
P. Costa**[1]**, F. Crescenzi**[1]**, A. Cucchiaro**[1]**, A. Doria**[1]**, G. Ferrò**[3]**, A. Gabrielli**[3]**,
S. Galeani**[3]**, C. Galperti**[6]**, P. Gasior**[9]**, E. Giovenale**[1]**, M. Gospodarczyk**[3]**,
L. Jakubowski**[10]**, M. Kubkowska**[9]**, A. Lampasi**[1]**, V. Lazic**[1]**, L. Lubyako**[11]**,
G. Maffia**[1]**, F. Martinelli**[3]**, J.R. Martin Solis**[12]**, F. Maviglia**[5]**, R. Mazzuca**[1]**,
M. Moneti**[8]**, F.P. Orsitto**[5]**, A. Palucci**[1]**, M. Passeri**[3]**, Z. Popovic**[12]**, C. Possieri**[3]**,
M. Rabinski**[10]**, S. Ratynskaia**[13]**, M. Reale**[1]**, S. Roccella**[1]**, M. Sassano**[3]**,
F. Starace**[1]**, P. Tolias**[13]**, A. Vertkov**[14]**, J. Zebrowski**[10] **and P. Zito**[1]

[1] ENEA, Fusion and Nuclear Safety Department, C.R. Frascati, Via E. Fermi 45, 00044 Frascati (Roma), Italy
[2] CNR, Istituto di Fisica del Plasma, Via R. Cozzi 53, 20125 Milano, Italy
[3] Dipartimento Di Ingegneria Civile e Informatica, Università di Roma Tor Vergata, Viale del Policlinico 1, 00133 Roma, Italy
[4] Consorzio RFX, Corso Stati Uniti 4, 35137 Padova, Italy
[5] Consorzio CREATE, Università di Napoli Federico II, Via Claudio 21, 80125 Napoli, Italy
[6] École Polytechnique Fédérale de Lausanne (EPFL), Swiss Plasma Centre (SPC), 1015 Lausanne, Switzerland
[7] Department of Electrical, Università di Catania, Electronics and Computer Engineering, 95125 Catania, Italy
[8] Centre for Research and Dissemination of Renewable Energy, Università della Tuscia, 01028 Orte, Italy
[9] Institute of Plasma Physics and Laser Microfusion, Warsaw, Poland
[10] National Centre for Nuclear Research, 7 Andrzeja Soltana Str., 05-400 Otwock, Poland
[11] Institute of Applied Physics, 46 Ulyanov St., Nizhny Novgorod, 603950, Russian Federation
[12] Universidad Carlos III de Madrid, Avenida de la Universidad 30, 28911 Madrid, Spain
[13] Space and Plasma Physics—KTH Royal Institute of Technology, SE-10044, Stockholm, Sweden
[14] JSC Red Star, Moscow, Russian Federation

CrossMark

Abstract

Since the 2016 IAEA Fusion Energy Conference, FTU operations have been mainly devoted to experiments on runaway electrons and investigations into a tin liquid limiter; other experiments have involved studies of elongated plasmas and dust. The tearing mode onset in the high density regime has been studied by means of the linear resistive code MARS, and the highly collisional regimes have been investigated. New diagnostics, such as a runaway electron imaging spectroscopy system for in-flight runaway studies and a triple Cherenkov probe for the measurement of escaping electrons, have been successfully installed and tested, and new capabilities of the collective Thomson scattering and the laser induced breakdown spectroscopy diagnostics have been explored.

Keywords: tokamak, overview, FTU

(Some figures may appear in colour only in the online journal)

1. Introduction

FTU is a compact high magnetic field machine (toroidal magnetic field B_T up to 8 T, plasma current I_p up to 1.6 MA) with circular poloidal cross-section (major radius $R_0 = 0.935$ m, minor radius $a = 0.30$ m) and metallic first wall. The stainless steel vacuum chamber has a thickness of 2 mm and is covered internally, at the high field side, by a toroidal limiter made of 2 cm thick molybdenum tiles, and a molybdenum poloidal limiter is also present at the low field side. Additional heating systems are available, namely a 140 GHz electron cyclotron (EC) system with power up to 1.5 MW and a 8.0 GHz lower hybrid system with power up to 2.0 MW [1]. In order to reduce the oxygen content, the FTU's walls are conditioned with a boron coating at the beginning of each experimental campaign. Since the 2016 IAEA Fusion Energy Conference in Kyoto, FTU operations were largely devoted to experiments on runaway electrons (REs) and liquid metal limiters. Other experiments have involved elongated plasmas, dust studies, the tearing mode (TM) onset in the high density regime and the highly collisional regimes. New diagnostics have been successfully installed and tested, and new capabilities of previously installed diagnostics have been explored.

2. Runaway electron studies

Post-disruption RE beam mitigation is one of the main concerns for ITER operations. RE beam control algorithms (Tore-Supra [2], DIII-D [3], FTU [4] and TCV [5]) for stabilization and current reduction can be combined with shattered pellet injection (SPI) and massive gas injection (MGI) and provide redundancy and backup in case of SPI/MGI failure. Stabilization and suppression of a post-disruption RE beam

has been tried on FTU, with a control architecture that allows detection of the current quench and its induction via the central solenoid and a controlled RE beam current ramp-down, where the beam is kept away from the vessel. The RE beam energy reduction is achieved [6], as confirmed by analyzing hard x-ray monitors and the runaway electron imaging spectroscopy (REIS) system that measures the synchrotron radiation emitted by REs (an estimation technique to retrieve the RE energy distribution function from REIS has been developed). The effectiveness of the proposed control scheme, also tested on TCV, has been discussed for ITER, where the control system should be able to maintain the RE beam for current quenches smaller than 4 MA.

Deuterium pellet and heavy material injections, by means of a laser blow-off (LBO) technique, have been performed both into steady-state flat-top pulses with REs and on post-disruption RE beams (figure 1), and data from the fast scanning CO_2-CO interferometer and spectroscopy diagnostics have been analyzed in order to study the dynamics of particle interaction with the RE beam and ionization to possibly extrapolate information for ITER predictions. Initial analyses have evidenced different types of instabilities in the presence of both thermal and cold background plasmas, and their correlation with the toroidal electric field and density is under investigation. Comparing the two kinds of instabilities evidenced in figure 1 (before and after 0.45 s, respectively), it is possible to see that in the first sequence of events the electron cyclotron emission (ECE) quickly decreases and recovers, and density peaks start at the ECE minima (figure 2, left side). In the second sequence, the ECE sharply rises, which is typical of the anomalous Doppler instability (also known as fan-instability), and density starts increasing during the instability and decays much more slowly than in the first sequence (figure 2,
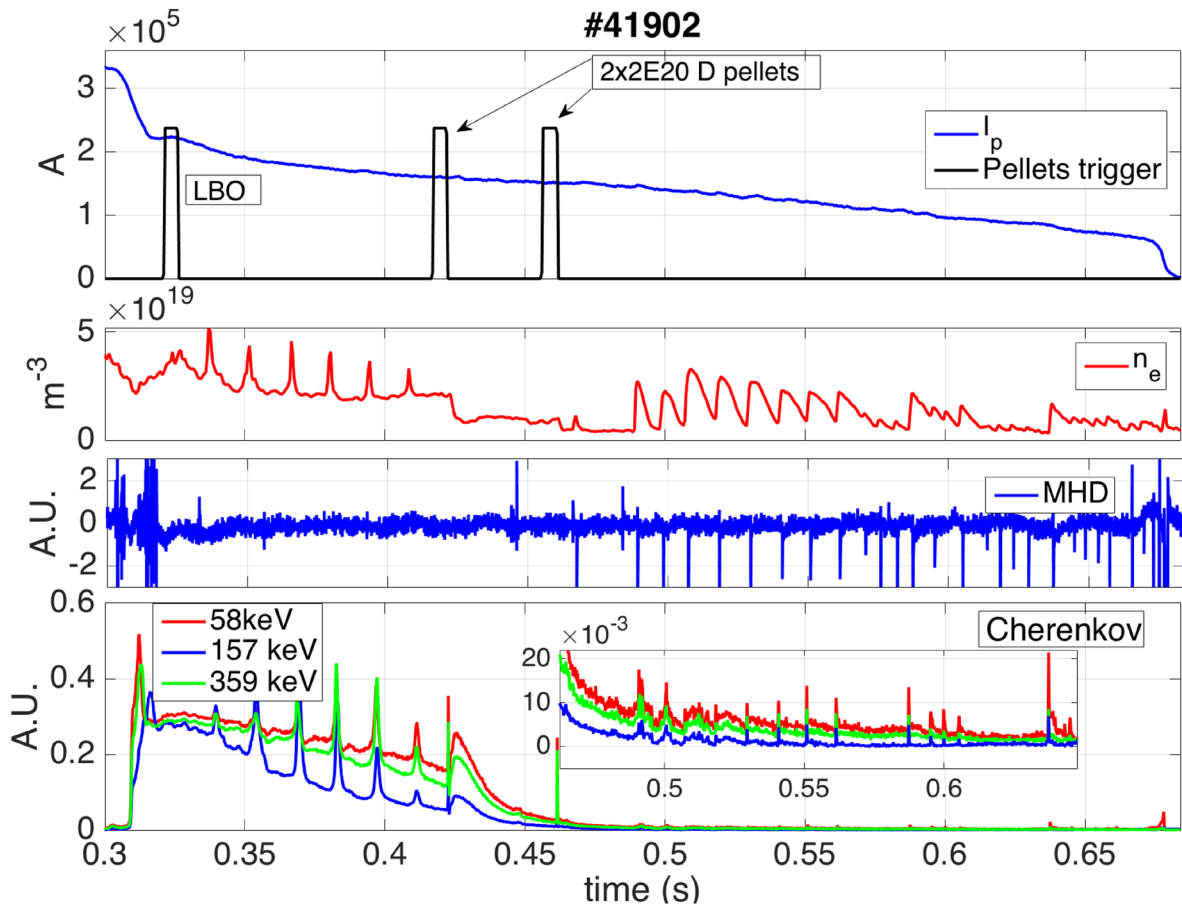
Figure 1. A post-disruption RE beam on which a first injection of iron with LBO followed by two deuterium pellets has been tested on a RE plateau. Electron density spikes are simultaneous to Cherenkov probe spikes, revealing that REs are expelled from the beam core due to instabilities, leading to gas recycling from the vessel. The origin of the RE expulsions after the iron injection is under investigation, whereas a sequence of fan-like instability events seems to take place after 0.45 s.
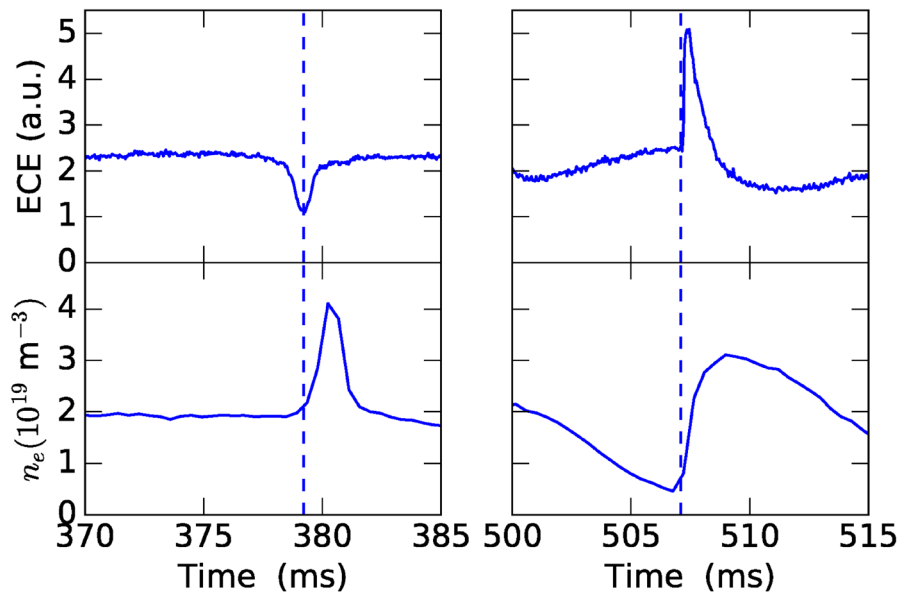

Figure 2. Upper frames: ECE at 300 GHz; lower frames: line-average density. Events from the first (second) sequence are shown at the left (right). Pulse #41902.
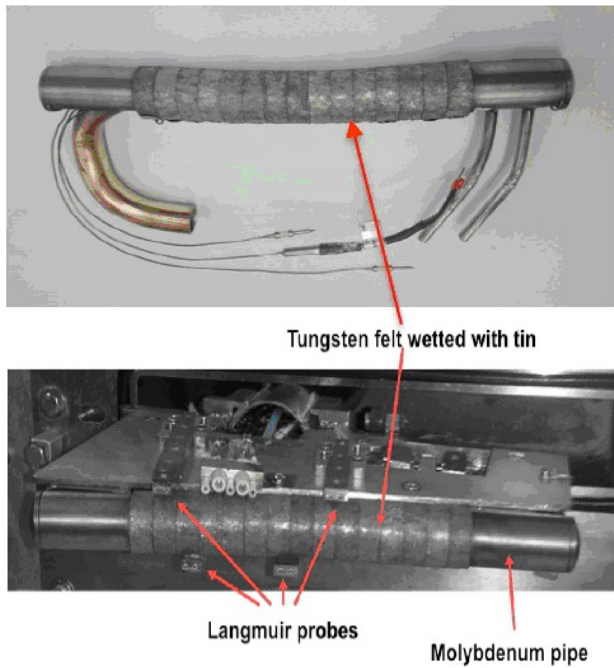
Tungsten felt wetted with tin

Langmuir probes

Molybdenum pipe

Figure 3. TLL installed on FTU. The TLL is equipped with several thermocouples and four Langmuir probes, two on each side.
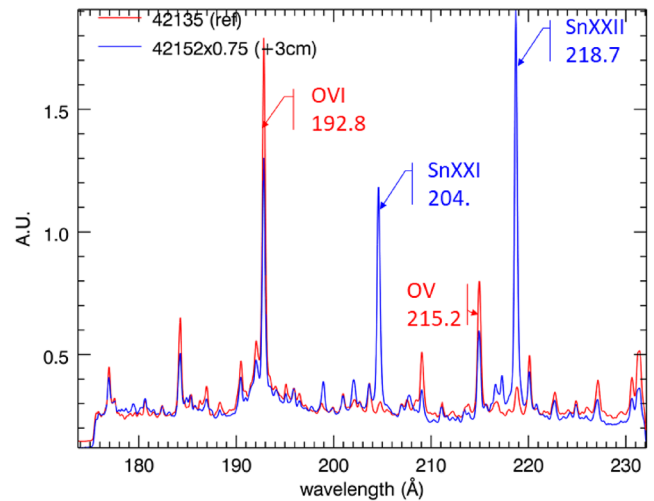

Figure 4. Comparison of one segment of the spectrum observed by the Schwob–Fraenkel XUV spectrometer for two pulses, one with the TLL fully retracted (in red), and the other with the TLL at $+3$ cm (in blue). The blue curve is normalized to the same background level.
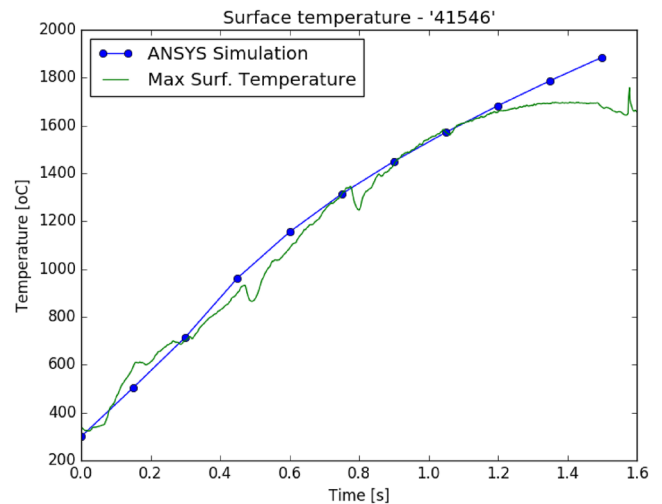

Figure 5. Experimental surface temperature compared with the ANSYS model. The flattening of the surface temperature can be linked to the evaporation phenomena.

right side). ECE has a fully non-thermal origin, in fact emission spectra are continuous, without any sign of the harmonics structure which characterizes thermal spectra. The spikes in the density plot after 0.45 s could be induced by gas recycling from the wall of expelled REs impacting the wall or ionizing the surrounding inert gas as discussed in [7]. The density spikes related to time lower than 0.45 s do not seem to be induced by known instabilities and are under study.

3. Tin liquid limiter experiments

In future fusion reactors, the divertor plates must not be subjected to average powers greater than 10 MW m^{-2}, with slow transients below 20 MW m^{-2}. More than 90% of the power will be radiated in the center and/or in the scrape-off layer (SOL), and the plasma will be partially detached. In this framework, liquid tin may prove a good candidate as a plasma facing component material, with a large operating window ($300 < T < 1300$ °C) before vaporization, low or negligible activation, and low H retention. Moreover, for $T > 1300$ °C, the thermal shield formed in front of the divertor plates by evaporated tin atoms can play an important role for power mitigation. Due to its high atomic number ($Z = 50$), tin meets the high core radiation requirement, but the maximum tolerable tin density for DEMO should be less than 10^{-3} of the electron density to be sustainable [8]. The tin liquid limiter (TLL) installed on FTU [9] (figure 3) is based on the innovative concept of the capillary porous system (CPS) [10]. It consists of a molybdenum tube, around which strips made of tungsten felt filled with tin are wrapped. To avoid hot spots in the intermediate region between the strips, the TLL head was realized with a bending radius ($r_{TLL} = 129$ cm) in the poloidal direction, much greater than the minor radius of the

plasma ($a = 30$ cm) in order to have a better and easier alignment of the CPS strips. The TLL can be cooled by flowing air and atomized water in a copper pipe inserted inside the molybdenum tube. The TLL limiter is equipped with several thermocouples and four Langmuir probes, two on each side. The surface temperature of the TLL limiter is recorded with a fast infrared (IR) camera observing the whole TLL surface from the top of the FTU machine (≈ 1 mm of spatial resolution and up to 1200 frames s^{-1} of acquisition rate). A 2 m grazing incidence Schwob–Fraenkel extreme ultraviolet (XUV) spectrometer [11] was installed on FTU observing the plasma emission in the range from 20 to 340 Å, to identify the spectral lines of Sn, with a high spectral resolution (figure 4).

The TLL (without active cooling) was carefully tested with standard FTU pulses at a toroidal magnetic field of $B_T = 5.3$ T, plasma current $I_p = 0.5$ MA and flat-top
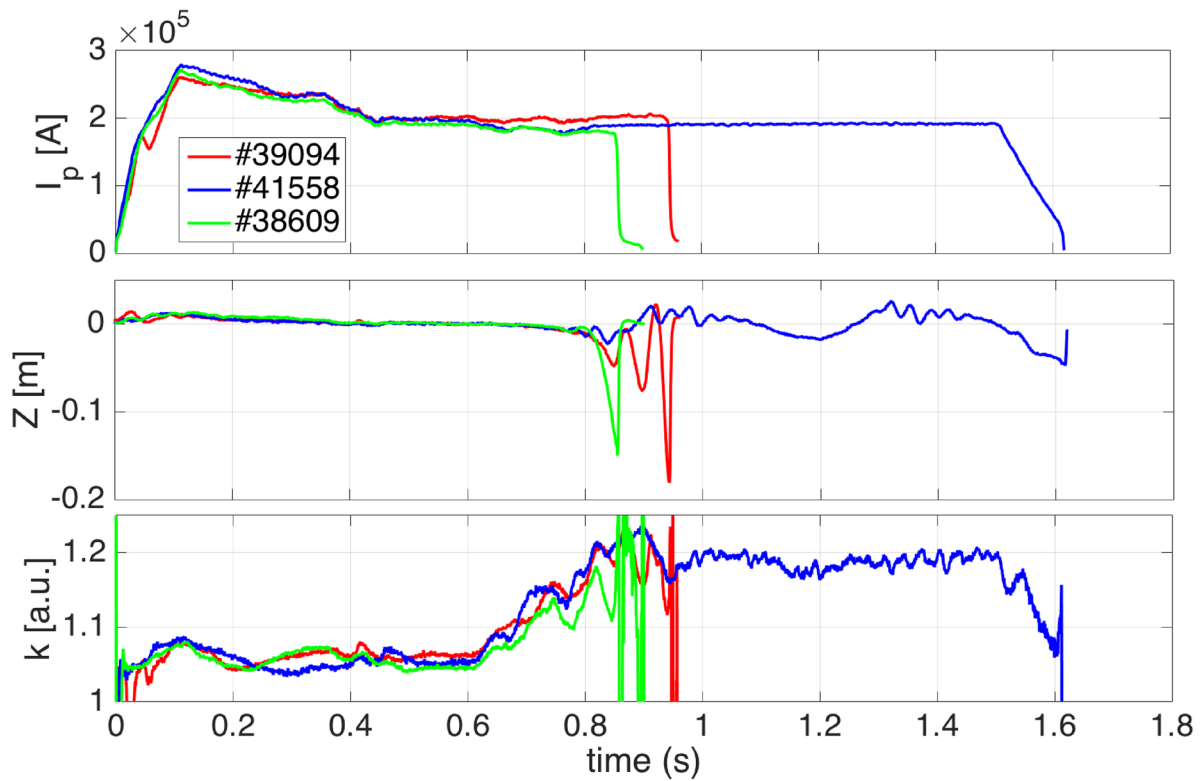
Figure 6. Comparison between the standard PID controller (red and green lines) and the new hybrid controller (blue lines). From top to bottom: plasma current I_p, vertical displacement z, and elongation k.

duration of 1.3 s, and the experimental results (obtained for the first time in the world in a tokamak with a TLL) have been carefully analyzed. The thermal load on the limiter was progressively varied moving up the limiter shot by shot into the SOL, until almost reaching the last closed magnetic surface (LCMS), and by increasing the electron density at a fixed limiter radial position (the electron temperature in the SOL of the FTU standard pulse of approximately 20 eV is almost independent of electron density). The maximum heat flux deduced by the Langmuir probes and the IR fast camera was about 18 MW m^{-2} for almost 1 s, for a TLL position closest to the LCMS. The maximum surface temperature measured by the IR fast camera on the tin limiter was approximately 1700 °C, reached at the end of the pulse. These results have been satisfactorily reproduced with the 3D finite-element code ANSYS, with a deviation of the measured Sn surface temperature from the simulated one only at the end of the pulse, which could be due to the development of a tin cloud (vapor shield) near the TLL (figure 5).

In particular, by looking at the temporal evolution of the IR maximum surface temperature and of the measured Sn XXI line emission monitored by the survey UV spectrometer SPRED, it was deduced that tin evaporation becomes the dominant tin production mechanism when the vapor pressure exceeds the plasma pressure [12]. It is worth pointing out that no droplets were observed entering into the plasma during the entire FTU experimental campaign and no damage was observed on the TLL after the plasma exposure. The effects on plasma performance were evaluated, especially when tin evaporation was dominant. A concentration of tin of about

5×10^{-4} of the electron density was deduced from the variation of the Z_{eff} value [13], under the assumption that it was due entirely to tin. The JETTO transport code [14] was used to compare two similar pulses with and without the tin limiter for the case in which tin evaporation was strong. The confinement time was practically the same within the error bars (10%–15%), without any degradation of the plasma performance.

4. Elongated plasmas

Preliminary experiments with elongated configurations were used on FTU to develop a proper elongation control [15]. Recently, a new hybrid vertical controller has been designed to stabilize vertically elongated plasmas in FTU, where vertical displacement events have been observed. The hybrid controller implements a logic described by differential equations and finite differences equations, so it is described by a double time, continuous and discrete (hybrid). In the latest experimental campaigns, experimental results showed its capability of stabilizing plasma up to the FTU record elongation of 1.23. As an example, a comparison between the standard proportional–integral–derivative (PID) controller and the new hybrid controller is reported in figure 6. In the pulses #39094 (red) and #38609 (green) the standard PID controller is considered and the pulses have been vertically lost. In contrast, when the hybrid controller has been introduced, the vertical confinement has been evidently improved as shown by the reported time traces (vertical displacement z and elongation k) of the pulse #41558 (blue). The parameter tuning

required three pulses, which is low if considered against other types of controller tuning. Further adaptive algorithms will be employed to extend control performances in case of long pulses. Elongated plasma pulses using the liquid metal limiters (lithium or tin) as the primary limiter is the subject of ongoing research.

5. Dust studies

Dust re-mobilization in tokamaks has been long recognized to be an issue affecting normal plasma operations. Evidence of the presence of an unexpected significant fraction of ferromagnetic dust in tokamak machines with both carbon fibre composite and full-metal walls are reported in the literature [16–18]. Magnetic dust particles, in contrast to non-magnetic ones, could be mobilized during, or even prior to, the pulse start-up, preventing a positive evolution or leading to an inhibition of the plasma pulse. To date not enough attention has been paid to these types of events with studies exclusively focusing on dust re-mobilization only after a full plasma pulse is established [19, 20]. Recent investigations on FTU proved the presence of dust mobilized prior to the pulse start-up phase, when in the tokamak volume the magnetic field consists just of the time-growing toroidal and multi-pole components due to the external coils. Evidence was provided by Thomson scattering (TS) and IR camera diagnostics triggered before the beginning of the pulses. In particular, TS spectra have shown the presence of dust in the chamber both before the ignition of the plasma pulse and during the sole magnetic field time evolution pulses (i.e. no plasma ignition) routinely used for diagnostic zeroing. An estimation of the dust concentration and size based on TS spectra and IR camera images indicated an average density of the order of 10^{-3} cm^{-3} and grain sizes between tens of μm and a few mm. Taking into account all possible origins of these observations, the only plausible explanation is the re-mobilization of magnetic dust present in the FTU vessel, due to the force applied by the magnetic field. A study of possible impacts of mobilized magnetic dust on tokamak operations has led to the conclusion that dust flying during the early stages of the pulse build-up could interfere primarily in three ways [21]: shifting the optimal loop-voltage versus gas pressure curve during the breakdown phase (shift in the Paschen curve), as a consequence of the reduced effective avalanche rate [22, 23] due to electron attachment to dust, inducing a delay up to a few 100 s ms in the plasma current ramp-up phase; perturbing the Z_{eff} and resistivity of plasma, limiting the flat top value of the current, for a given loop-voltage; and inducing disruptions when the full plasma is established due to the evaporation of massive grains of high Z magnetic dust that could be present right in the plasma core. All of these three mechanisms depend on the actual dust density in the vessel. There are several factors which might determine the actual dust density in a given FTU plasma pulse. We could mention the nature of the experimental campaigns, the cleaning of the vessel at the beginning of the experimental campaign and the history of the previous pulses (in particular, the presence of current disruptions or

REs). As a topical example, we can mention the occurrence of high current ($I_p > 0.5$ MA) plasma disruption that, usually, drastically increases the dust density in the following pulse. Therefore, the average dust density value reported in this section should be assumed as merely indicative because it could drastically vary from pulse to pulse in the same experimental day.

6. Tearing mode analysis with the MARS code

A TM is an instability that arises in magnetically confined plasma as a consequence of the plasma finite resistivity. It develops on q rational surfaces and it is driven by the radial gradient of the toroidal current density. A detailed study on TMs has been carried out in the contest of high density regimes, where the magnetic perturbation associated with the mode can increase up to disruption [24, 25]. When the density increases, an increase of the radiation losses is also observed which leads to a contraction of the temperature profile and so to shrinkage of the current profile. Because the TM is driven by the radial gradient of the current, as the current shrinks, TMs appear in the experimental pulse. The onset of the TMs during FTU pulses has been analyzed by means of the MARS code [26], which is a global, resistive, spectral code for full magnetohydrodynamic (MHD) linear stability analysis. With this aim, the temporal evolution of the pulse has been reconstructed from the experimental data with the JETTO transport code [14]. The equilibria obtained at different times were then translated into the CPOs (consistent physical objects) data environment [27], thus making them suitable for reading by a high-resolution equilibrium code solver such as CHEASE [28]. Indeed, it is worth noting that both the CHEASE and the MARS codes are fully compliant with the EUROfusion WPCD (work package code development for integrated modelling) CPOs environment and, recently, they have been ported to the IMAS [29] environment as well.

The linear stability of a sufficient number of FTU pulses has been analyzed in the high density regimes with different plasma currents I_p (from 500 kA to 900 kA) and different toroidal magnetic fields B_T (from 4 T to 8 T). The onset of the TM, established by the MARS code simulations, has been compared with the one observed experimentally from magnetic pick-up coil signals and a good agreement can be claimed. In figure 7 one single analyzed pulse (#34769) is shown as an example. On the left-hand side the experimental evolution of the central line-averaged density and of the derivative of the perturbed poloidal magnetic field are shown and the vertical dashed lines correspond to the analyzed times (the black dotted line corresponds to the experimental onset of the TM). On the right-hand side the growth rate (normalized to the Alfvén time τ_A) of the mode for the different analyzed times (from 0.75 s to 1.25 s), and thus different equilibria, is shown as a function of the inverse Lundquist number $1/S$. Here vertical lines represent the experimental inverse Lundquist number at a certain time; of course, if the vertical line intercepts the growth rate curve (coloured circles), the mode is unstable, vice versa it is stable. In the figure, instability is
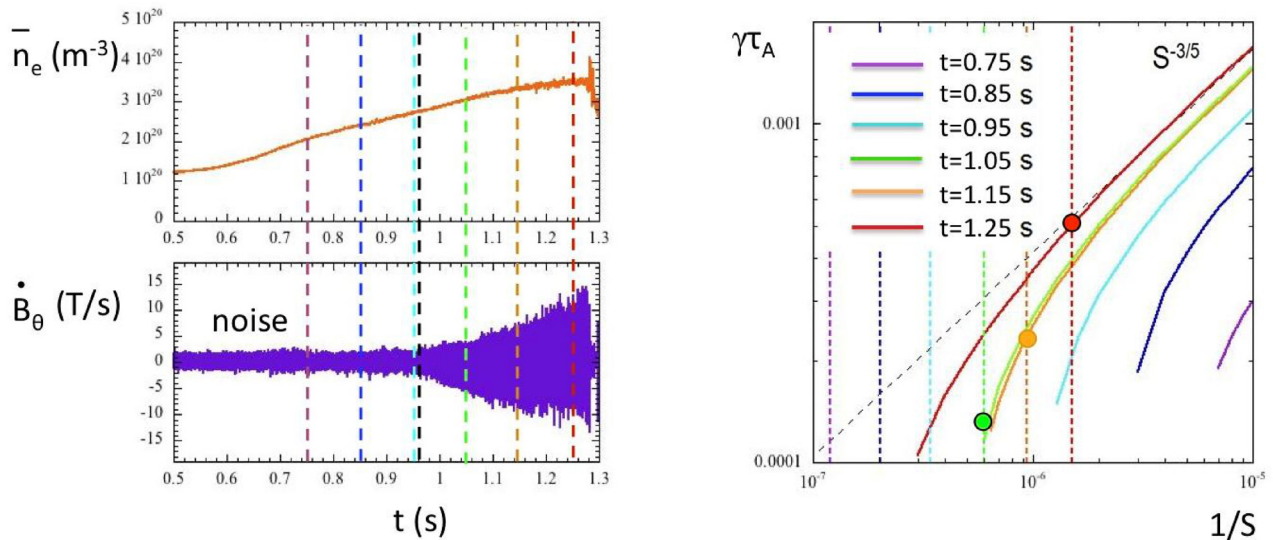
Figure 7. FTU pulse #34769. $B_T = 8$ T, $I_p = 900$ kA. (Left) Temporal evolution of the central line-averaged density and of the derivative of the perturbed poloidal magnetic field. (Right) MARS output for different times (equilibria) during the density ramp-up, the effective values of the experimental inverse Lundquist number are shown as vertical dotted lines. The coloured circles on these lines individuate the intercepts with the MARS solutions.

observed for analyzed times greater or equal than 1.05 s (green dotted line), which can be compared to the experimental onset found around 0.96 s (black dotted line in the figure on the left-hand side). Note that the curve bending of the growth rate is due to the curvature effect; indeed, additional simulations have been performed with MARS progressively reducing the plasma pressure (therefore also the curvature effect). In this case, besides increasing the growth rate at high $1/S$ values, the curve bending at low $1/S$ values also disappears and the mode always becomes unstable in the considered time window. Finally, MARS results have been validated with convergence tests on the mesh size, the number of spectral components and the mesh packaging around the rational q surfaces.

7. Highly collisional regimes

In literature an inverse linearity between the electron density peaking and the effective collisionality ν_{eff} is found for most tokamak devices [30], as reported in figure 8 for pulses with ν_{eff} from 0.2 to 10 (grey symbols). FTU offers the unique opportunity to explore regimes of high collisionality (up to ~100), thanks to the capability to operate up to very high electron density values. In particular, it has been observed that the inverse linearity of the density peaking versus the effective collisionality is similar to other devices at low and medium collisionality (JET, Asdex, JT-60U, and Alcator C-Mod, although in the H-mode regime). However, at high values of collisionality such inverse linearity does not occur, but, instead, an increase of the density peaking with the collisionality is found, as reported in figure 8 (red symbols).

In particular, from the comparison between pulses with and without the MARFE instability and with lithium or boron wall conditioning, it seems that the increase of the density peaking is related to edge phenomena, as in the MARFE instability presence [24] and ameliorated conditioning of wall by using
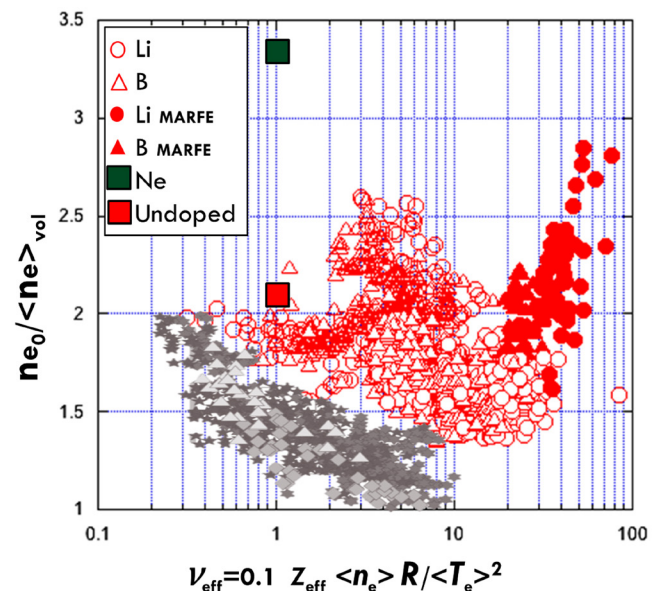

Figure 8. Density peaking as a function of the effective collisionality. Red symbols for FTU data; grey symbols for other devices. The behaviour of a neon doped pulse on FTU is also reported (green square).

the lithium limiter [31]. In these cases, plasmas of particular interest in terms of density peaking are observed. Another interesting effect is associated with the neon injection [32]: keeping the same collisionality, an impressive increase of the density peaking is obtained for doped pulses with respect to the un-doped ones.

8. Diagnostics

Since the 2016 IAEA Fusion Energy Conference in Kyoto, new diagnostics, such as a REIS system for in-flight runaway
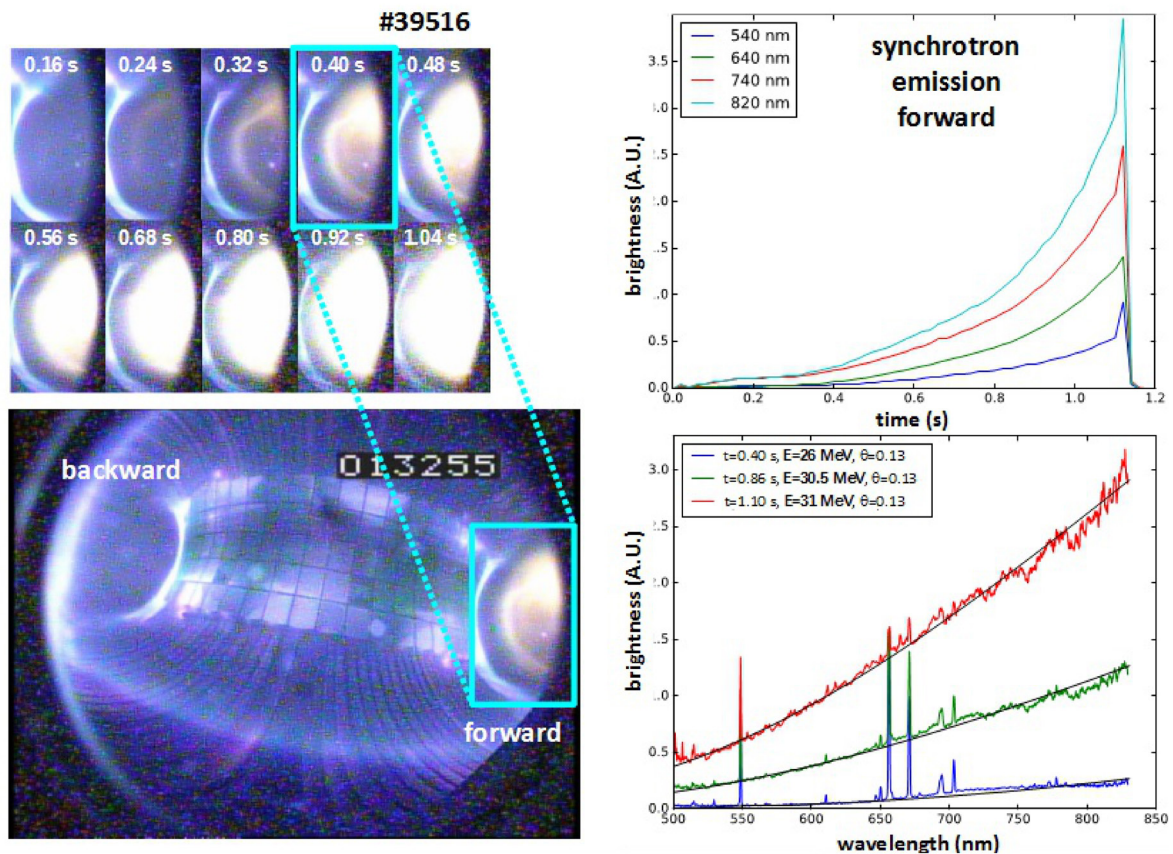
Figure 9. Pulse #39516. Visible camera images of the RE beam (left): the bottom image (corresponding to frame 013255, $t = 0.4$ s) shows both RE backward and forward views, while the top image is a time sequence of the forward view for the same pulse. Note the temporal correlation of the visible images with the measured synchrotron radiation intensity at several wavelengths (top right) and synchrotron radiation spectra (bottom right). In particular, the spectra are fitted (solid lines) assuming mono-energetic distributions (energy and pitch angle values in the insert).

studies and a triple Cherenkov probe for the measurement of escaping electrons, have been successfully installed and tested, and new capabilities of the collective TS and the laser induced breakdown spectroscopy (LIBS) diagnostics have been explored.

8.1. Runaway electron imaging spectroscopy

The REIS system, developed to detect images and spectra of synchrotron emission from in-flight REs, was calibrated and commissioned as a portable diagnostic for operation in a medium sized tokamak. First operated in FTU, after design and construction of suitable interfaces, the REIS was installed in ASDEX Upgrade and TCV and exploited in RE generation and control experiments. The REIS system is a wide-angle optical diagnostics collecting RE synchrotron radiation from two plasma cross sections (corresponding to RE backward and forward views) and transmitting it to visible/IR spectrometers via an incoherent bundle of fibers. The present operating spectral range spans from 0.3 to 2.5 μm, and it will be extended to 5 μm in a major re-design and upgrade. As an example of the information provided by the REIS diagnostics, for the FTU pulse #39516, in which REs are already generated in the very early stages of the pulse, in figure 9 images of the RE beam from the visible camera (left) are shown and correlated

with the measured synchrotron radiation intensity at several wavelengths (top right) and the measured synchrotron radiation spectra (bottom right). The spectra are fitted (black solid lines) using formula (1) from [33] for a mono-energetic RE distribution. It is worth noting that the measured energy and pitch angle values (see insert in figure 9, bottom right) are in agreement with the predictions of simulations based on a test particle model of the RE dynamics [34]: the calculated RE energy distribution gradually becomes mono-energetic with a maximum energy of ∼30 MeV.

8.2. Cherenkov probe

Predicting and controlling plasma disruptions in tokamaks is one of the key features for a reliable application of nuclear fusion. In particular, measurements of fast electrons produced in the plasma core and escaping from it are of interest to study processes occurring inside the plasma itself. A Cherenkov diagnostic is a good candidate to perform these studies and both single and triple Cherenkov probes were installed on FTU and their performances have been under investigation [35]. In particular, the triple probe differs from the single one for the fact that it has three diamond detectors with three different energy thresholds (58, 187 and 359 keV), thus it is able to perform a first energy scan. Each diamond detector is
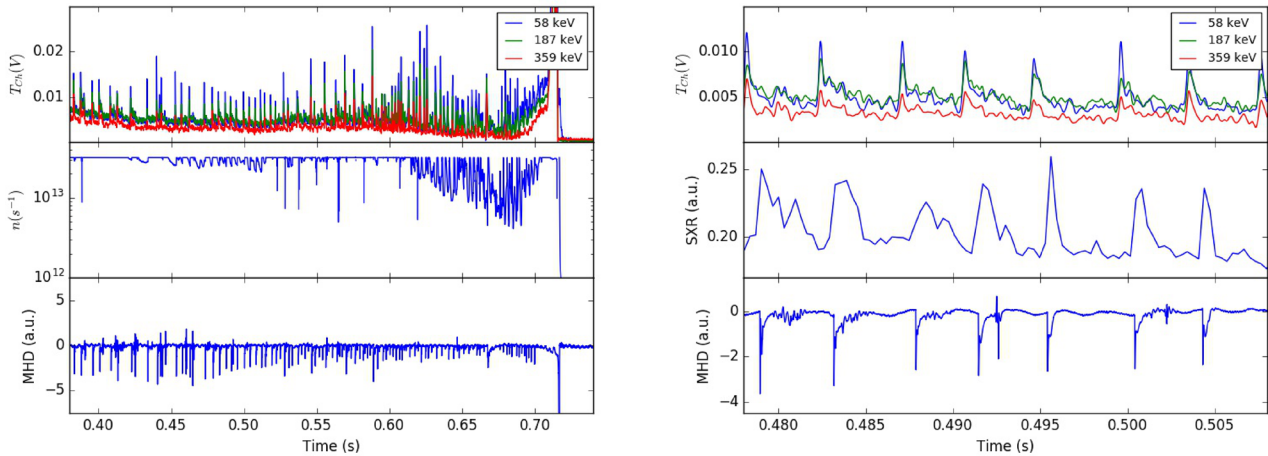
Figure 10. (Left) Correlation between triple Cherenkov probe signal, gamma-ray count rate and MHD activity. (Right) Triple Cherenkov signal, soft x-rays and MHD activity. Pulse #41146.

mounted on a titanium zirconium molybdenum (TZM) head inserted into the FTU vessel, and it is coated with a Ti/Pt/Au inter-layer filtering out visible light, particularly the plasma D_α line. In the triple probe, two of them have a further deposition of Mo, respectively 56 μm and 164 μm in order to have different threshold energies. Electrons impinging on the probe emit Cherenkov radiation in diamond, and this radiation is routed, through a visible/ultraviolet optical fiber, to a PMT operating at high voltage (1 kV) with a detectable range of 185–850 nm.

An example of analysis focusing on the capability and sensitivity of the probes to measure RE losses with energy discrimination in the presence of perturbations due to kinetic reconnection phenomena is described in the following, confirming the Cherenkov probe to be a valid diagnostic system to study and monitor plasma scenarios involving REs generation. The anomalous Doppler effect (ADE), also known as fan instability, is a kinetic instability that tends to transfer energy from parallel (with respect to magnetic field *B*) to perpendicular particle motion. Figure 10 (left) shows an example, with a comparison between Cherenkov signals, gamma-ray emission rate and magnetic activity. During plasma pulse #41146 RE expulsion due to the ADE appeared in the ramp-down phase driven by a soft-stop (active control activates when a safety threshold value on a hard x-ray signal is exceeded for more than 10 ms). The most notable thing is the correlation of each peak from x-rays and Cherenkov signals to those from the MHD activity, also visible on a smaller scale on figure 10 (right). At this time scale, it is seen that these peaks rapidly rise up in just a few μs. Note, moreover, that the Cherenkov peaks are clean and more distinct than those from the x-ray signals, due to the better time resolution of the probes. Regarding the thresholds, the blue signal dominates (58 keV), followed by the green (187 keV) and the red one (359 keV). This shows that, during this pulse, fan instability generates expulsion of REs with energies in general smaller than those usually observed.

8.3. Collective Thomson scattering (CTS) diagnostics

The CTS diagnostic allows the investigation of ion populations in fusion plasma devices, studying the characteristic emissions, stimulated by the injection of a powerful microwave probing beam. From the shape of the emitted spectrum, plasma parameters such as ion temperature, drift velocity and ion composition can be inferred [36, 37]. The availability in FTU of a CTS diagnostic system at 140 GHz and the possibility of 'non-resonant' plasma scenarios, i.e. scenarios in which the EC layer (and harmonics) resonant with the probe frequency are out of the plasma region, allow for studies on ion characteristics [38]. In fact, in the presence of EC resonances, the ECE background (at a probing frequency) can significantly overwhelm the signals due to thermal CTS. Nevertheless, in recent experiments, the CTS diagnostics were also used for investigations on parametric decay instability excitation by EC beams in correlation with magnetic islands induced by neon injection and in resonant scenarios [39, 40]. Parasitic emissions from the gyrotron were observed, while other spectral emissions (lines and bands) have been observed and analyzed with very high time and frequency resolution. To determine the mechanism of emissions and locate the plasma volume generating them, an independent receiving line has been recently installed.

8.4. Laser induced breakdown spectroscopy (LIBS)

The quantitative detection of tritium retained in ITER in vessel components is mandatory for deciding if the machine operation must be stopped and the excessive tritium removed. LIBS is a suitable and non-invasive *in situ* diagnostic for detecting retained tritium; in particular, the multi-purpose deployer, a robotic arm which can be installed on ITER during maintenance, could be equipped with a LIBS system to analyze a consistent area of the vessel. In the last year, LIBS measurements of deuterium (used as a proxy for tritium) retained in, and the surface elemental composition of, the FTU molybdenum
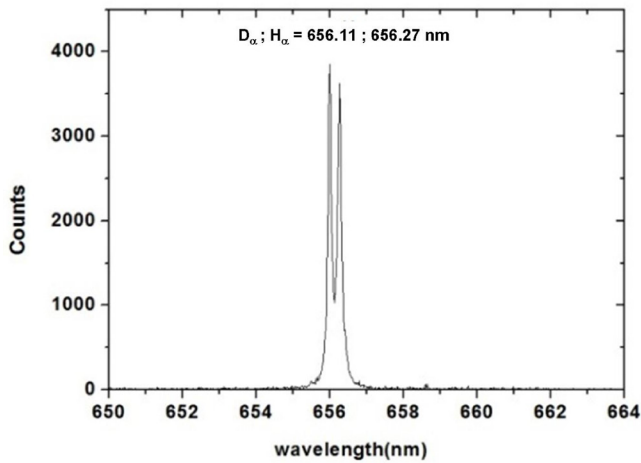
Figure 11. Deuterium and hydrogen emission lines detected by LIBS on a shadowed zone in between the FTU toroidal limiter tiles.

(TZM) toroidal limiter tiles, have been carried out remotely (~2.5 m) during machine maintenance [41], with measurements performed both in vacuum and in nitrogen or argon atmospheres. The main goal of the experiments was to verify the feasibility of retained deuterium detection for supporting the proposed use of a robotic arm for an extended LIBS analysis of the in-vessel FTU components.

The experimental layout consisted of a Quantel laser 'Twin BSL' ($\lambda = 1064$ nm), a Andor 'Istar DH320T-18F-63' intensified charge-coupled device camera with a 1024×512 sensor (26 μm pixels) and a Jobin Ivon 'Triax 550' spectrometer (550 mm) with a 2400 grooves mm^{-1} grating. A single pulse technique has been used. The collinear transmission of the laser beam and detection of emitted visible lines was done through the 2 inch window of an equatorial port by using a dielectric mirror. Laser and optics for laser transmission and visible lines detection were mounted on a plate movable along three axes and able to be pivoted. Vacuum measurements resulted in a good resolution of D_α and H_α emission lines (figure 11) and in the detection, besides molybdenum, the main component of the TZM alloy, of lithium coming from the lithium deposited during the experiments with a lithium limiter, inserted in the vessel through a vertical port located 60° toroidally apart. Deuterium was also detected in the shadowed zones in between tiles. Measurements carried out at atmospheric pressure showed different results depending on the used gas, nitrogen or argon. With nitrogen (1000 mbar), no evident deuterium and hydrogen emission lines were detected. The limited available experimental time did not allow for a deep analysis of the causes: a possible explanation is the partial formation of NH and ND compounds, of which the emission lines in the LIBS plasma plume were not detectable in our experiments given the cut of emitted line wavelengths below 400 nm, caused by the dielectric mirror. With the argon atmosphere (500 mbar) the deuterium and hydrogen emission lines were well visible although with a worse resolution with respect to the vacuum measurements, as was expected because of the larger Stark broadening of emitted lines. After a fresh boron treatment (routinely performed in FTU by using deuterated diborane) deuterium was also detected together with boron lines, therefore reproducing, at least partially, the ITER situation, where tritium is foreseen to be retained in the machine mainly by co-deposition with beryllium.

9. Conclusions

Stabilization and suppression of a post-disruption RE beam has been achieved on FTU, with a control architecture that allows for detection of the current quench and its induction via the central solenoid using a controlled RE beam current ramp-down, where the beam is kept away from the vessel. Initial analyses have evidenced different types of instabilities in the presence of both thermal and cold background plasmas, and their correlation with the toroidal electric field and density is under investigation. The TLL was tested with standard FTU pulses ($B_T = 5.3$ T, $I_p = 0.5$ MA); the maximum thermal load deduced by the Langmuir probes was about 18 MW m^{-2} for almost 1 s, without any degradation of the plasma performance, proving liquid tin to be a good candidate as a plasma facing component material. A 2 m grazing incidence Schwob–Fraenkel XUV spectrometer was installed on FTU observing the plasma emission in the range from 20 to 340 Å, to identify the spectral lines of Sn, with high spectral resolution, during the TLL experiments. A new vertical controller has been designed to stabilize vertically elongated plasmas in FTU, where vertical displacement events have been observed. Experimental results showed its capability of stabilizing plasma up to the FTU record elongation of 1.23. Recent investigations on FTU proved the presence of dust mobilized prior to the pulse start-up phase, when in the tokamak volume the magnetic field consists only of the time growing toroidal and multi-pole components due to the external coils. The onset of TM in the high density regime has been analyzed by means of the MARS code, which is a global, resistive, spectral code for full MHD linear stability analysis. The obtained onset times have been compared with the ones observed experimentally from magnetic pick-up coil signals and a good agreement can be claimed. An increase of the density peaking with the effective collisionality ν_{eff} has been found on FTU at high values of ν_{eff}. This behaviour seems to be related to edge phenomena, as in the MARFE instability presence and ameliorated conditioning of wall by using the lithium limiter.

The REIS diagnostic has allowed the simultaneous provision of the image and the visible/infrared spectrum of the forward and backward radiation from in-flight REs. A triple Cherenkov probe was installed and tested on FTU, confirming the Cherenkov prove to be a valid diagnostic system to study and monitor plasma scenarios involving REs. The CTS diagnostics were used for investigations on parametric decay instability excitation by EC beams in correlation with magnetic islands induced by neon injection. Parasitic emissions from the gyrotron were observed, while other spectral emissions have been observed and analyzed. LIBS measurements of the deuterium retained on the FTU molybdenum toroidal limiter tiles have shown that LIBS is a suitable, non-invasive, *in situ* diagnostic for quantitative detection of tritium retained in the ITER vessel components.

References

[1] Gormezano C. *et al* 2004 *Fusion Sci. Technol.* **45** 297
[2] Saint-Laurent F. *et al* 2011 *European Conf. Abstracts: Proc. 38th EPS Conf. on Plasma Physics (Strasbourg, France, 27 June–1 July 2011)* vol 35G O3.118 (http://ocs.ciemat.es/EPS2011PAP/pdf/O3.118.pdf)
[3] Hollmann E.M. *et al* 2013 *Nucl. Fusion* **53** 083004
[4] Esposito B. *et al* 2017 *Plasma Phys. Control. Fusion* **59** 014044
[5] Carnevale D. *et al* 2017 *European Conf. Abstracts: Proc. 44th EPS Conf. on Plasma Physics (Belfast, Northern Ireland, UK, 26–30 June 2017)* vol 41F P1.152 (http://ocs.ciemat.es/EPS2017PAP/pdf/P1.152.pdf)
[6] Carnevale D. *et al* 2019 *Plasma Phys. Control. Fusion* **61** 014036
[7] Paz-Soldan C. *et al* 2019 *Plasma Phys. Control. Fusion* **61** 054001
[8] Poradzinski M. *et al* 2017 *Fusion Eng. Des.* **124** 248
[9] Vertkov A. *et al* 2017 *Fusion Eng. Des.* **117** 130
[10] Vertkov A. *et al* 2007 *Fusion Eng. Des.* **82** 1627
[11] Schwob J.L. *et al* 1987 *Rev. Sci. Instrum.* **58** 1601
[12] van Eden G.G. *et al* 2017 *Nat. Commun.* **8** 192
[13] Bombarda F. *et al* 2018 *European Conf. Abstracts: Proc. 45th EPS Conf. on Plasma Physics (Prague, Czech Republic, 2–6 July 2018)* vol 42A P1.1005 (http://ocs.ciemat.es/EPS2018PAP/pdf/P1.1005.pdf)
[14] Cenacchi G. and Taroni A. 1986 *Proc. 8th Eur. Conf. Compounds Physics (Eibsee)* vol 10D p 57
[15] Ramogida G. *et al* 2017 *Nucl. Mat. Energy* **12** 1082
[16] Ivanova D. *et al* 2009 *Phys. Scr.* **T138** 014025
[17] Novokhatsky A.N. *et al* 2011 *European Conf. Abstracts: Proc. 38th EPS Conf. on Plasma Physics (Strasbourg, France, 27 June–1 July 2011)* vol 35G P5.066 (http://ocs.ciemat.es/EPS2011PAP/pdf/P5.066.pdf)
[18] De Angeli M. *et al* 2015 *Nucl. Fusion* **55** 123005
[19] Tolias P. *et al* 2016 *Plasma Phys. Control. Fusion* **58** 025009
[20] Ratynskaia S. *et al* 2016 *Nucl. Fusion* **56** 066010
[21] De Angeli M. *et al* 2019 private communication
[22] Pedersen A. 1967 *IEEE Trans. Power Syst.* **86** 200
[23] Loeb L.B. and Meek J.M. 1941 *The Mechanism of the Electric Spark* (Palo Alto, CA: Stanford University Press)
[24] Pucella G. *et al* 2013 *Nucl. Fusion* **53** 083002
[25] Pucella G. *et al* 2013 *European Conf. Abstracts: Proc. 40th EPS Conf. on Plasma Phys. (Espoo, Finland, 1–5 July 2013)* vol 37D P5.139 (http://ocs.ciemat.es/EPS2013PAP/pdf/P5.139.pdf)
[26] Bondeson A. *et al* 1992 *Phys. Fluids* B **4** 1889
[27] Imbeaux F. *et al* 2010 *Comput. Phys. Commun.* **181** 987
[28] Lutjens H. *et al* 1996 *Comput. Phys. Commun.* **97** 219
[29] Imbeaux F. *et al* 2015 *Nucl. Fusion* **55** 123006
[30] Angioni C. *et al* 2009 *Plasma Phys. Control. Fusion* **51** 124017
[31] Mazzitelli G. *et al* 2011 *Nucl. Fusion* **51** 073006
[32] Mazzotta C. *et al* 2015 *Nucl. Fusion* **55** 073027
[33] Stahl A. *et al* 2013 *Phys. Plasmas* **20** 093302
[34] Popovic Z. *et al* 2016 *Phys. Plasmas* **23** 122501
[35] Causa F. *et al* 2015 *Nucl. Fusion* **55** 123021
[36] Stejner M. *et al* 2015 *Plasma Phys. Control. Fusion* **57** 062001
[37] Stejner M. *et al* 2011 *Plasma Phys. Control. Fusion* **53** 065020
[38] Bin W. *et al* 2016 *Rev. Sci. Instrum.* **87** 11E507
[39] Bruschi A. *et al* 2017 *Nucl. Fusion* **57** 076004
[40] Baiocchi B. *et al* 2018 *J. Instrum.* **13** C07006
[41] Maddaluno G. *et al* 2019 *Nucl. Mater. Energy* **18** 208